01 Jan 2023

Thermal and Electrical Properties of Spark Plasma Sintered (Ti,cr)b2 Ceramics

Steven M. Smith

Lun Feng

William Fahrenholtz
Missouri University of Science and Technology, billf@mst.edu

Gregory E. Hilmas
Missouri University of Science and Technology, ghilmas@mst.edu

et. al. For a complete list of authors, see https://scholarsmine.mst.edu/matsci_eng_facwork/2861

Recommended Citation

S. M. Smith et al., "Thermal and Electrical Properties of Spark Plasma Sintered (Ti,cr)b2 Ceramics," *Journal of the American Ceramic Society*, vol. 106, no. 1, pp. 632 - 638, Wiley, Jan 2023.
The definitive version is available at https://doi.org/10.1111/jace.18791

Received: 20 July 2022 | Revised: 7 September 2022 | Accepted: 8 September 2022

DOI: 10.1111/jace.18791

Journal of American Ceramic Society

RESEARCH ARTICLE

Thermal and electrical properties of spark plasma sintered (Ti,Cr)B_2 ceramics

Steven M. Smith II[1] | **Lun Feng**[1] | **William G. Fahrenholtz**[1] | **Gregory E. Hilmas**[1] | **Laura Silvestroni**[2]

[1]Materials Science and Engineering Department, Missouri University of Science and Technology, Rolla, Missouri, USA

[2]CNR-ISTEC, Institute of Science and Technology for Ceramic Materials, Faenza, Ravenna, Italy

Correspondence
Steven M. Smith II, Materials Science and Engineering Department, Missouri University of Science and Technology, Rolla, MO, USA.
Email: smsqn9@mst.edu

Funding information
North Atlantic Treaty Organization, Grant/Award Number: MYP-G5767

Abstract

Thermal and electrical properties were measured for TiB_2 ceramics containing varying CrB_2 contents up to 33 mol%. The room-temperature thermal diffusivity decreased with increasing Cr content from 0.330 ± 0.003 cm^2/s for pure TiB_2 to 0.060 ± 0.003 cm^2/s for $(Ti_{0.66}Cr_{0.33})B_2$. The amount of anisotropy in the coefficients of thermal expansion increased with increasing Cr content and the *c*-axis had the greatest dependence on Cr addition, with an increase of more than 25% in the thermal expansion for 33 mol% CrB_2 compared to TiB_2, whereas the *a*-axis only increased by about 8%. The electrical conductivity was the lowest for $(Ti_{0.66}Cr_{0.33})B_2$ at ~8.5×10^3 S/cm compared to ~106.1×10^3 S/cm for nominally pure TiB_2. Overall, the addition of CrB_2 as a sintering aid for TiB_2 was shown to have a significant effect on the thermal and electrical properties of TiB_2 for additions as small as 5 mol% CrB_2.

KEYWORDS
electrical conductivity, titanium diboride, thermal conductivity, thermal expansion

1 | INTRODUCTION

TiB_2 is an ultrahigh temperature ceramic (UHTC) due to its melting point (>3200°C).[1] Compared to other UHTCs, TiB_2 has a lower theoretical density (4.50 g/cm^3) and higher hardness (~25 GPa at 9.81 N) that make it an appealing material for several engineering applications.[2] However, achieving high relative densities is difficult as sintering of TiB_2 is usually accompanied by strong grain growth, which combined with the anisotropic thermal expansion, results in microcracking for grain sizes >15 μm.[2,3] As a result, sintering aids are often added to preserve a fine microstructure and promote densification. Common sintering aids for TiB_2 include SiC, B_4C, TiC, $MoSi_2$, Si_3N_4, and $TiSi_2$ that typically result in the presence of a second phase in the final ceramics.[4–9] CrB_2 is another potential sintering aid and has been shown to form a complete solid solution with TiB_2, making it an attractive additive.[10] The use of solid-solution additives may promote a retention of elevated temperature properties of the final ceramic.

CrB_2 and TiB_2 both form a hexagonal (AlB_2-type) crystal structure, with CrB_2 also possessing a low theoretical density of 5.20 g/cm^3.[11] In contrast, CrB_2 has a lower ratio of the c/a values of coefficients of thermal expansion (CTE) than TiB_2 (0.91 compared to 1.46 for TiB_2)[3] and is not considered a UHTC (T_m ~ 2200°C).[10] For hot-pressed CrB_2 with relative densities ranging from 84% to 92%, the thermal conductivity was reported to be 534 ± 40 cal/(s cm K) (~22 ± 2 W/m K) at room temperature.[12] CrB_2 single crystals have been previously studied to determine their magnetic and electrical properties.[13,14] Tanaka et al. and later Bauer et al. measured the electrical resistivity to be in the range of ~60–100 $\mu\Omega$ cm (electrical conductivity of 1.00–1.67 × 10^4 S/cm) depending on the crystallographic direction.[13,14] In polycrystalline CrB_2, it is likely that the

electrical resistivity would be at the higher end of the range due to the presence of porosity as well as grain boundaries, which was shown by Farrior[15] and Kislyi et al.[12] who reported electrical resistivities of ~90 $\mu\Omega$ cm for an 80% dense sample and $84 \pm 5\,\mu\Omega$ cm for samples 84%–92% dense for polycrystalline CrB_2.

Transport properties of pure TiB_2 have also been studied, including thermal diffusivity, thermal conductivity, and electrical resistivity. NIST[2] reports a thermal diffusivity of 0.30 ± 0.02 cm^2/s and thermal conductivity of 96 ± 6 W/m K at room temperature for TiB_2 with a relative density of ≥98%. Typical values for the electrical resistivity of TiB_2 can range from ~7 to 40 $\mu\Omega$ cm at room temperature and are dependent on the relative density.[15–17] Transport properties of TiB_2–$MoSi_2$ ceramics showed variance as a function of $MoSi_2$ content; however, the ceramics were not of single phase, which leads to extrinsic effects. The $MoSi_2$ study showed that the thermal diffusivity of the ceramics decreased with $MoSi_2$ content over 2.5 wt%, with ~0.24 cm^2/s for pure TiB_2 and ~0.22 cm^2/s for 10 wt% $MoSi_2$ at room temperature.[7]

Previous studies showed that some properties of TiB_2 could be improved by producing $(Ti,Cr)B_2$ solid-solution ceramics. Feng et al.[18] reported that $(Ti_{0.9}Cr_{0.1})B_2$ had an increased relative density of 99.6% compared to pure TiB_2 at 97.9% under the same sintering conditions. Additionally, they were able to maintain a similar hardness, reporting 36.7 ± 4.3 GPa for pure TiB_2 and 35.3 ± 4.2 GPa for the Cr addition at 0.981 N. Murthy et al.[19] studied CrB_2 additions of 2.5, 5, and 10 wt% (2.4, 4.7, and 9.5 mol%), reporting that the 2.5 wt% addition had the highest relative density (96.6% compared to 89% for pure TiB_2), but they did not report the resulting grain size for that composition. In the same study, a bulk of CTE and electrical resistivity for the 10 wt% CrB_2 composition was also reported to be 6.82×10^{-6} K^{-1} at 298–473 K and 32.83 $\mu\Omega$ cm at room temperature, respectively.

The present study reports the thermal and electrical properties of $(Ti,Cr)B_2$ ceramics by examining the thermal diffusivity/conductivity, crystallographic thermal expansion, and electrical resistivity of TiB_2 with varying CrB_2 contents from 0 to 33 mol%.

2 | EXPERIMENTAL PROCEDURES

Chromium oxide (Cr_2O_3, 99.5%, 0.7 μm; Elementis), titanium oxide (TiO_2, 99.9%, 32 nm APS; Alfa Aesar), and boron carbide (B_4C, 96.8%, 0.6–1.2 μm; HC Starck) were used as starting materials. $(Ti_{1-x}Cr_x)B_2$ compositions (TCB-*X*) were synthesized by the boro/carbothermal synthesis process reported by Feng et al.[18] Target additions of CrB_2 were up to 25 mol%, but the nomenclature used for the final ceramics uses X as the CrB_2 content in the final ceramics determined by energy-dispersive spectroscopy (EDS, INCA Energy 300, Oxford Instruments). For the present study, the reaction time at 1650°C was adjusted to 2.5 h. The reacted powders were then crushed and collected for sintering and testing.

The reacted powders were densified into 20 or 40 mm graphite dies that were lined with graphite foil and densified by spark plasma sintering (DCS10, Thermal Technology) using the schedule previously reported by Feng et al.[18] Theoretical densities were calculated based on the batched composition and lattice parameters determined by Rietveld refinement of the X-ray diffraction (XRD) patterns of the densified samples. Relative densities were calculated from these theoretical densities and the measured bulk densities using the Archimedes method.

Field-emission scanning electron microscopy (SEM, ΣIGMA, ZEISS) was used to gather images of each sintered sample of TCB-*X* for grain size analysis. EDS was used to determine the composition of sintered samples, and the reported values are an average of at least five grains from two areas of each sample. Computerized image processing software (ImageJ, National Institutes of Health) was used to determine average grain size by measuring at least 400 grains for each sample.

Measurement of the CTE was done by variable temperature XRD (X-Pert MPD, Philips) on the synthesized powders. Reacted powders were passed through a 200-mesh sieve and mixed thoroughly with magnesium oxide powder (MgO, electronic grade, 99.5% <20 μm; Fisher Scientific) as an internal standard. The MgO was calcined in air at 1073 K for 3 h to decompose any carbonate and/or hydroxide species. The powder mixture was loaded onto a sapphire disk and then placed on a platinum strip heater. XRD patterns were collected for all TCB-*X*/MgO mixtures under flowing nitrogen at temperatures from 298 to 1073 K in 100 K steps. Resulting patterns were then analyzed by Rietveld refinement to determine the lattice parameters of both the TCB-*X* and MgO phases at each temperature. The MgO lattice parameters were used to determine the actual temperature of the samples. MgO is cubic and has a volumetric CTE characterized by Saxena et al.[20] that varies with temperature by Equation (1). Once the temperature was determined from the MgO lattice parameters, the relative differences between the room-temperature lattice parameters and the lattice parameters at each temperature of the TCB-*X* powders were analyzed using a linear regression fit, with the slope of the line being the CTE of the powder

$$\alpha = 3.754 \cdot 10^{-5} + 7.907 \cdot 10^{-9}T - 0.7836T^{-2} + 0.9148T^{-3} \quad (1)$$

TABLE 1 Nominal energy-dispersive spectroscopy (EDS) composition, grain size, lattice parameter aspect ratio, c/a coefficients of thermal expansion (CTE) ratio, and density of sintered TCB-X ceramics

Sample	TiB_2 (mol%)	CrB_2 (mol%)	Grain size (μm)	c/a ratio	CTE c/a ratio	Relative density (%)	Theoretical density (g/cm^3)
TCB-0	100	0	24.7 ± 17.3	1.066	1.435	97.4	4.48
TCB-0.06	94.0	6.0	7.8 ± 3.2	1.064	1.559	98.6	4.53
TCB-0.10	89.7	10.3	4.6 ± 1.9	1.062	1.555	99.1	4.57
TCB-0.19	80.9	19.1	5.5 ± 2.3	1.058	1.556	98.2	4.61
TCB-0.26	74.4	25.6	7.5 ± 3.1	1.056	1.759	98.3	4.65
TCB-0.33	67.4	32.6	6.2 ±2.8	1.054	1.682	99.3	4.69

The thermal diffusivity was measured on the sintered ceramics. The samples were manually surface ground to remove any reaction layer, and electrical discharge machining (EDM, Agiecut 150) was used to cut the samples into ~12.7 mm disks. Resulting disks were then coated with a thin layer of graphite to promote uniform energy absorption during testing. A thermal property analyzer (Flashline L-S2, Anter Corporation) was used to measure the thermal diffusivity of each sample from ~298 to 473 K by the laser-flash method, taking measurements approximately every ~25 K. The measured values of thermal diffusivity were used, along with bulk densities from Archimedes' measurements and estimated heat capacities to calculate the thermal conductivity using in the following equation:

$$\kappa = DC_p\rho_r \tag{2}$$

where κ is thermal conductivity (W/m K), D is thermal diffusivity (cm^2/s), C_p is heat capacity (J/kg K), and ρ_r is the measured density. Densities were assumed to be constant in this temperature range, and heat capacity was estimated using a volumetric rule of mixtures based on the compositions determined by EDS and heat capacity values of TiB_2 and CrB_2 from a thermodynamic software package (FactSage, Version 8.1, ThermFact Inc. and GTT-Technologies).

Electrical resistivity measurements were first made on sintered specimens of each composition. Bars of each composition were cut by EDM to dimensions of $2 \times 2.4 \times 23$ mm^3 and then machined to $1.5 \times 2 \times 23$ mm^3. A four-point probe technique was conducted using an in-house fixture (KEITHLEY 2230G-30-1 power source) at a 20 V maximum and a constant 0.01 A current. Resistivity was calculated by Equation (3) where ρ is the resistivity, A is the cross-sectional area of the bar (cm^2), Δ is the distance between the inner probes (cm), Ω is the calculated resistance ($\mu\Omega$), V_Δ is the measured voltage drop between the inner probes (μV), and I is the applied amperage (A). Electrical conductivity was calculated as the inverse of the electrical resistivity:

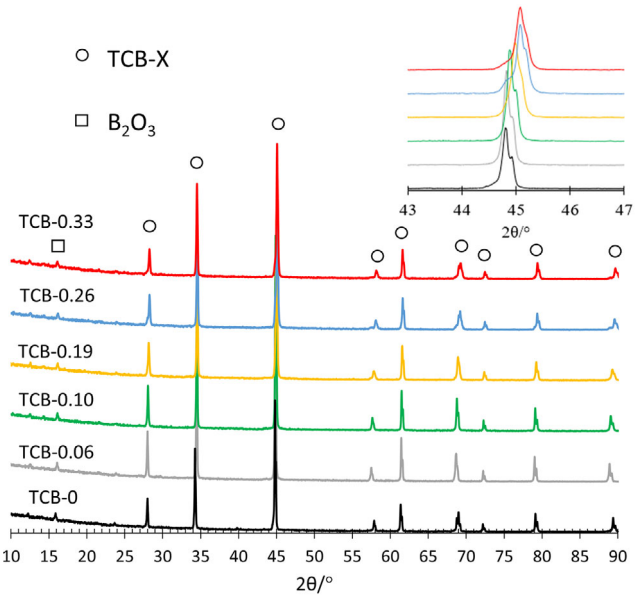

FIGURE 1 X-ray diffraction (XRD) patterns for the TCB-X powder samples. The enlarged view around 45° shows a shift to the right with increasing Cr content dissolved into the TiB_2 lattice.

$$\rho = \frac{A}{\Delta}\Omega = \frac{A}{\Delta} \cdot \frac{V_\Delta}{I} \ (\mu\Omega\,\text{cm}) \tag{3}$$

3 | RESULTS AND DISCUSSION

3.1 | Microstructural and compositional characterization

Composition, average grain size, lattice parameter aspect ratio, and Archimedes densities for each densified sample are summarized in Table 1. Room-temperature XRD patterns for the TCB-X powders only had peaks for the TCB-X phase and a small peak attributed to B_2O_3 formed from surface oxidation, as shown in Figure 1. The powders all appeared to form a single boride phase after reaction at 1650°C for 2.5 h. As shown in the inset, the peaks shifted

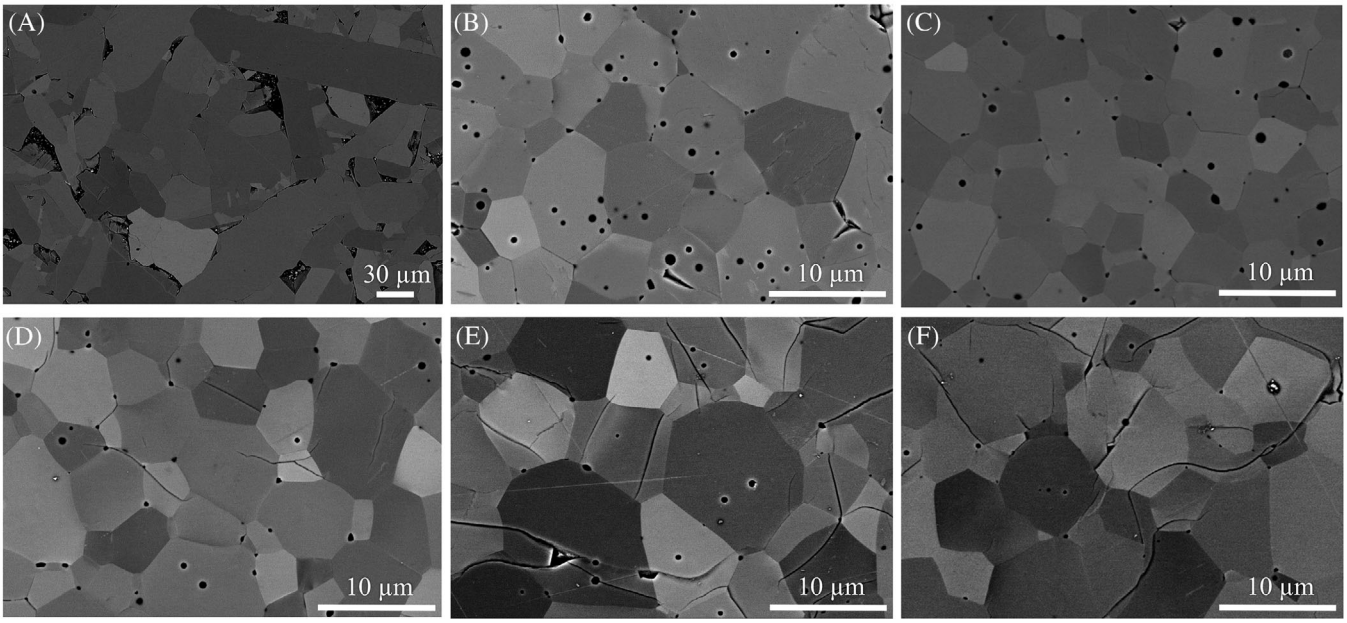

FIGURE 2 Scanning electron microscopy (SEM) micrographs of (A) TCB-0, (B) TCB-0.06, (C) TCB-0.10, (D) TCB-0.19, (E) TCB-0.26, and (F) TCB-0.33

to higher angles with increasing Cr content due to the smaller size of Cr compared to Ti.

SEM micrographs of each sintered composition are shown in Figure 2. All samples had relative densities >97%. The grain size of TCB-0 was ~24.7 μm with the grain sizes of all other compositions in the 4.6–7.8 μm range. No clear trend with composition could be identified. Grain elongation along the preferential axis was suppressed with the smallest Cr addition. A small volume fraction of porosity was trapped inside the grains for all Cr additions and decreased with increasing Cr content, with trapped porosity ranging from 0.8 vol% for TCB-0.06 to 0.1 vol% for TCB-0.33. Microcracking can be seen for CrB_2 additions greater than 10 mol%, and visibly increase with increasing Cr content. No secondary phases were observed by SEM. The apparent contrast in the images was based on grain orientation that resulted from electron channeling. Based on EDS analysis, the compositions of the resulting ceramics were different from the batched compositions. The TCB compositions all appeared to be enriched in Cr compared to the nominal batched compositions, which is likely due to loss of TiO_2 during the powder synthesis. The subsequent analysis in the present paper utilizes the compositions that were measured by EDS.

3.2 | Coefficient of thermal expansion

The CTEs of each composition are plotted in Figure 3 as a function of Cr content over the temperature range 298–873 K. The measured CTEs of TCB-0 were similar to those

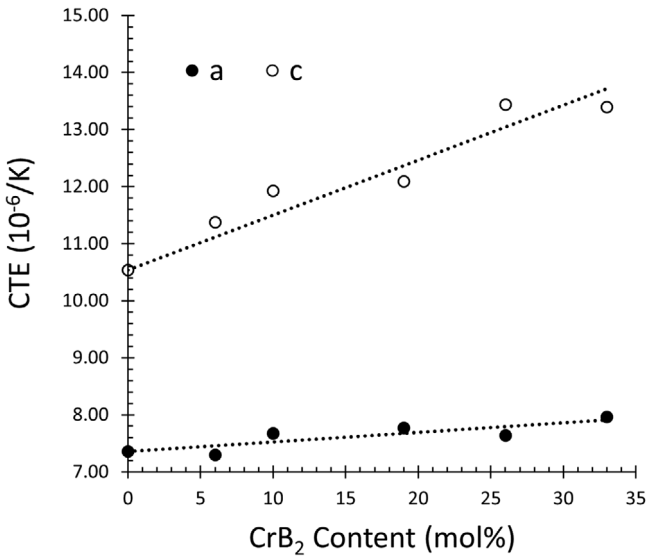

FIGURE 3 The crystallographic coefficients of thermal expansion (CTE) from 298 to 873 K graphed as a function of Cr content as measured by energy-dispersive spectroscopy (EDS)

reported for TiB_2 by NIST[2] for this temperature range for the a (7.36×10^{-6} K^{-1}) and c (10.54×10^{-6} K^{-1}) axes. The difference between CTE in the a and c directions indicates anisotropy between the crystallographic directions with a c/a ratio of 1.44 for TCB-0. As Cr content increased, the CTE values for both the a and c directions increased roughly linearly with composition, but the magnitudes of the changes were different for the two directions. The CTE for the c-axis had the stronger dependence on Cr content.

The CTE in this direction is controlled by the strength of the metal–B bonds and indicates that Cr–B bonds are weaker than Ti–B bonds due to the increase in CTE with Cr content. The CTE along the *a*-axis is controlled by the B–B bonds, which are not as strongly affected by changes in Cr content as the bonds in the *c* direction.

The *c*/*a* CTE ratio was used to characterize the change in the anisotropy of the CTE. As Cr content increased, the CTE in the *c* direction increased more than that in the *a*-direction, which indicated an increase in CTE anisotropy with Cr additions (Table 1). The CTE in the *a*-direction increased from 7.36×10^{-6} K^{-1} for TCB-0 to 7.96×10^{-6} K^{-1} for TCB-0.33, which was an increase of only ~8%. In contrast, the CTE for the *c* direction increased by ~27% from TCB-0. A previous study by Okamoto et al. showed that CrB_2 had less CTE anisotropy than TiB_2, which suggested that the *c*/*a* CTE ratio should have decreased with the addition of Cr.[3] However, CTE anisotropy increased with Cr additions in the present study. The increase in the *c*/*a* CTE ratio with increasing Cr content also explains the increase in microcracking observed for TCB-0.26 and TCB-0.33 compared to lower Cr contents, Figure 2.

3.3 | Thermal diffusivity and conductivity

The thermal diffusivity of TCB-0 was 0.330 ± 0.003 cm^2/s at 293 K, which is similar to the thermal diffusivity reported by NIST[2]. At the same temperature, the thermal diffusivity of TCB-0.33 was the lowest, 0.060 ± 0.003 cm^2/s. Figure 4A shows that the room-temperature thermal diffusivity of the TCB-*X* samples decreased with increasing Cr content, which resulted in a decrease in thermal diffusivity of about 60% at 293 K. The decrease in thermal diffusivity with Cr additions is expected because the substitution of Cr in the Ti–Ti sublattice distorts the lattice and promotes phonon scattering. This behavior is also seen in other borides like $(Zr,M)B_2$ ceramics where differences in valency and bonding affected the measured thermal diffusivities.[21,22] Additionally, the increase in microcracking with Cr content can also reduce thermal diffusivity. Further additions of Cr had a lesser effect on thermal diffusivity than the initial addition and the diffusivity approached a value of ~0.05 cm^2/s as Cr content increased. Figure 4B shows the temperature dependence of the thermal diffusivity. The thermal diffusivity decreased with increasing temperature due to increased phonon scattering from inherent lattice vibration.

Thermal conductivity values for the TCB-*X* samples are shown in Figure 5. The thermal conductivity of TCB-0 was 93.5 ± 0.1 W/m K at 298 K. For the addition of Cr, thermal conductivity ranged from ~37 to 18 W/m K at 298 K. The decrease in thermal conductivity is a direct result of the reduction in thermal diffusivity as Cr content increased. The thermal conductivity also stabilized with the addition of Cr with only a ~0.4% difference for TCB-0.10 over this temperature range, whereas there was a ~19% difference for TCB-0. This stabilization was also a result of increased phonon scattering and/or microcracking due to the addition of Cr.

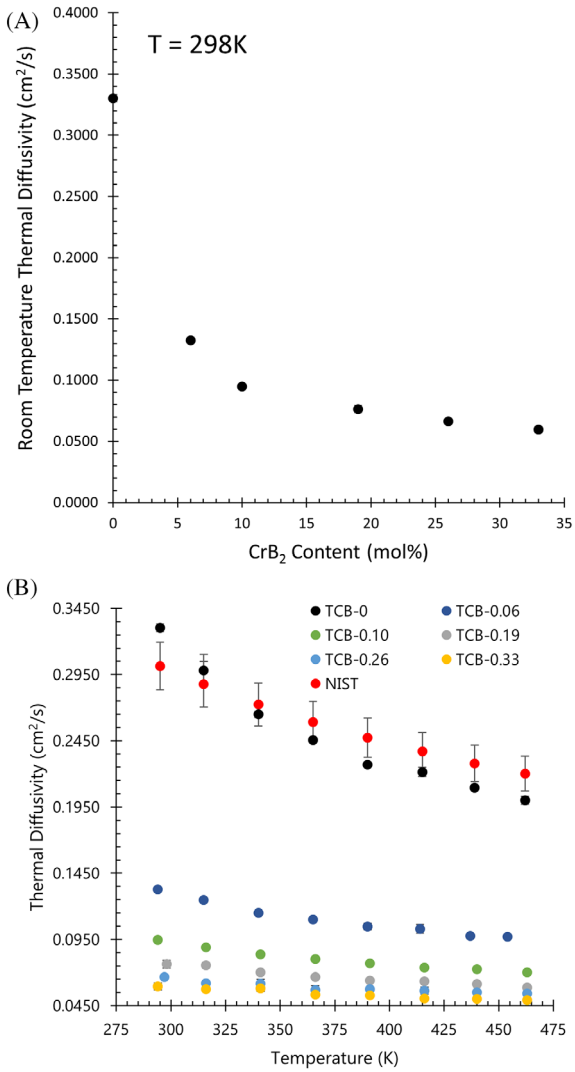

FIGURE 4 (A) The room-temperature thermal diffusivity as a function of CrB_2 content and (B) the thermal diffusivity of the TCB-*X* ceramics as a function of temperature up to 475 K

3.4 | Electrical resistivity and conductivity

The room-temperature electrical resistivity and conductivity for each composition are shown in Figure 6. The electrical conductivity was ~1.07×10^5 S/cm for TCB-0 and decreased to ~8.5×10^3 S/cm for TCB-0.33. The electrical

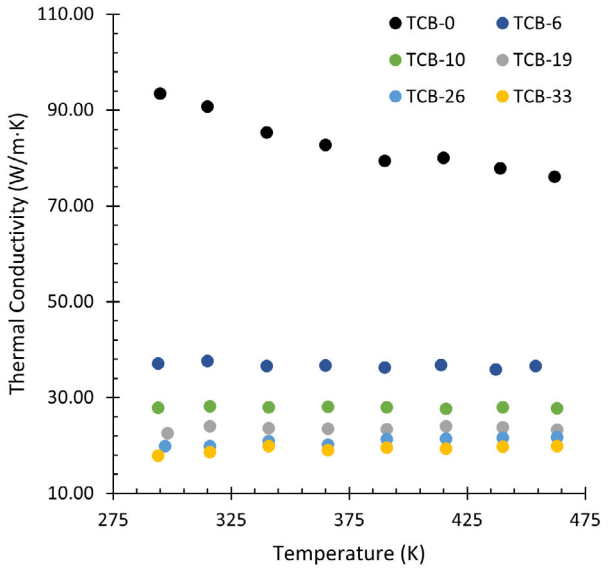

FIGURE 5 The thermal conductivity of TCB-*X* ceramics

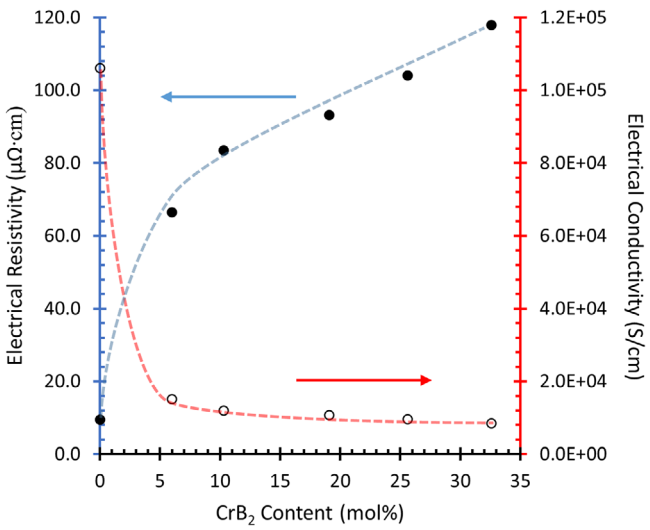

FIGURE 6 Electrical resistivity and conductivity of the TCB-*X* samples at room temperature

resistivity/conductivity changed sharply from TCB-0 to 0.06 but changed less as CrB_2 content increased. The values of electrical resistivity are shown for comparison to published studies. For example, the electrical resistivities measured in the present study were approximately an order of magnitude lower than reported by Farrior[15] for the same range of compositions due to the increased relative density in the present study (>97% in the present study compared to ~80% for Farrior).

The decrease in electrical conductivity with increasing Cr content was caused by increased electron scattering due to the addition of Cr and the introduction of microcracking that has previously been shown to reduce electrical conductivity in TiB_2 ceramics.[23] The electrical conductivity decreased with both the 6 and 10 mol% additions even without microcracking, which suggests that the microcracking present for higher amounts of Cr was not the only cause of the decrease in electrical conductivity. If the microcracking could be reduced, then the electrical conductivity may be increased. The decrease in electrical conductivity with Cr addition also indicated that Cr affected the electronic contribution to the thermal conductivity. Based on this analysis, the addition of Cr affected both the electron and phonon contributions to the thermal conductivity, which explains the overall change in thermal conductivity with Cr addition.

4 | CONCLUSIONS

Thermal and electrical properties were determined for high density $(Ti,Cr)B_2$ ceramics with CrB_2 contents ranging from 0 to 33 mol%. Variable temperature XRD revealed that the crystallographic CTEs of TiB_2 were 7.36×10^{-6} K^{-1} for the *a*-axis and 10.54×10^{-6} K^{-1} for the *c*-axis over the range of 298–873 K. The addition of Cr in solid solution increased both crystallographic CTEs and increased the degree of anisotropy of the thermal expansion due to differences between the strengths of Ti–B and Cr–B bonds. The thermal diffusivity decreased from 0.330 cm^2/s for TiB_2 to ~0.054 cm^2/s for $(Ti_{0.94}Cr_{0.06})B_2$ due to the increases in phonon and electron scattering that resulted from Cr addition. The addition of CrB_2 also stabilized the temperature dependence of the thermal conductivity. The electrical conductivity was significantly affected by the initial 6 mol% CrB_2 content, which resulted in a ~86% decrease in electrical conductivity from pure TiB_2, with steady decreases for higher Cr contents. The present study showed that CrB_2 can be a potential sintering aid for TiB_2 ceramics; however, contents as low as 6 mol% CrB_2 are enough to significantly reduce the thermal and electrical conductivities of TiB_2 and additions greater than 10 mol% can induce microcracking, which would negatively affect mechanical properties.

ACKNOWLEDGMENTS

This research was sponsored by the NATO Science for Peace and Security Program under Grant number: MYP-G5767 (SUSPENCE). The authors would like to acknowledge Dr. Eric Bohannan at Missouri S&T for his assistance with XRD and Dr. Carlo Baldisserri at ISTEC for his assistance with electrical measurements.

ORCID

Steven M. Smith II https://orcid.org/0000-0002-2179-4060

William G. Fahrenholtz https://orcid.org/0000-0002-8497-0092

Laura Silvestroni https://orcid.org/0000-0003-4595-0299

REFERENCES

1. Wuchina EJ, Opila E, Opeka MM, Fahrenholtz WG, Talmy IG. UHTCs: ultra-high temperature ceramic materials for extreme environment applications. Electrochem Soc Interface. 2007;16(30):30–6.
2. Munro RG. Material properties of titanium diboride. J Res Natl Inst Stand Technol. 2000;105(5):709–20.
3. Okamoto NL, Kusakari M, Tanaka K, Inui H, Otani S. Anisotropic elastic constants and thermal expansivities in monocrystal CrB_2, TiB_2, and ZrB_2. Acta Mater. 2010;58:76–84.
4. Neuman EW, Brown-Shaklee HJ, Hilmas GE, Fahrenholtz WG. Titanium diboride-silicon carbide-boron carbide ceramics with super-high hardness and strength. J Am Ceram Soc. 2018;101:497–501.
5. Yan SR, Foong LK, Lyu ZJ. Technical performance of co-addition of SiC particulates and SiC whiskers in hot pressed TiB_2-based ultrahigh temperature ceramics. Ceram Int. 2020;46:19443–51.
6. Ismail AE, Alimin AJ, Mohd Tobi AL, Khalid A, Abdullah HZ, Masood I, et al. Fabrication of TiB_2-TiC composites optimized by different amount of carbon in the initial Ti-B-C powder mixture. Appl Mech Mater. 2013;315:720–3.
7. Raju GB, Basu B, Suri AK. Thermal and electrical properties of TiB_2-$MoSi_2$. Int J Refract Met Hard Mater. 2010;28:174–9.
8. Park J, Koh Y, Kim H, Hwang CS. Densification and mechanical properties of titanium diboride with silicon nitride as a sintering aid. J Am Ceram Soc. 1999;82(11):3037–42.
9. Raju GB, Basu B. Densification, sintering reactions, and properties of titanium diboride with titanium disilicide as a sintering aid. J Am Ceram Soc. 2007;90(11):3415–23.
10. Telle R. The quasi ternary system TiB_2-CrB_2-WB_2 between 1500 and 1900°C and the related quasi binary subsystems. J Eur Ceram Soc. 2019;39(13):3677–83.
11. Okada S, Kudou K, Iizumi K, Kudaka K, Higashi I, Lundstrom T. Single-crystal growth and properties of CrB, Cr_3B_4, Cr_2B_3 and CrB_2 from high-temperature aluminum solutions. J Cryst Growth. 1996;166:429–35.
12. Kislyi PS, L'vov SN, Nemchenko VF, Samsonov GV. Physical properties of the boride phases of chromium. Poroshkovaya Metallurgia. 1962;6(12):50–3.
13. Tanaka T, Nozaki H, Bannai E, Ishizawa Y, Kawai S, Yamane T. Preparation and properties of CrB_2 single crystals. J Less-Common Met. 1976;50:15–21.
14. Bauer A, Regnat A, Blum CGF, Gottlieb-Schonmeyer S, Pedersen S, Meven M, et al. Low-temperature properties of single-crystal CrB_2. Phys Rev B. 2014;90:064414.
15. Farrior G. Diborides in the pseudobinary system TiB_2-CrB_2: electrical properties. U.S. Department of the Interior Bureau of Mines; 1965. p. 1–26.
16. Rahman M, Wang CC, Chen W, Akbar SA, Mroz C. Electrical resistivity of titanium diboride and zirconium diboride. J Am Ceram Soc. 1995;78(5):1380–2.
17. McLeod AD, Haggerty JS, Sadoway DR. Electrical resistivities of monocrystalline and polycrystalline TiB_2. J Am Ceram Soc. 1984;67(11):705–8.
18. Feng L, Fahrenholtz WG, Hilmas GE, Silvestroni L. Superhard single-phase $(Ti,Cr)B_2$ ceramics. J Am Ceram Soc. 2022;105:5032–8.
19. Murthy TSRCh, Sonber JK, Subramanian C, Fotedar RK, Gonal MR, Suri AK. Effect of CrB_2 addition on densification, properties and oxidation resistance of TiB_2. Int J Refract Met Hard Mater. 2009;27:976–84.
20. Saxena SK, Zhang J. Thermochemical and pressure-volume-temperature systematics of data on solids, examples: tungsten and MgO. Phys Chem Miner. 1990;17(1):45–51.
21. McClane DL, Fahrenholtz WG, Hilmas GE. Thermal properties of $(Zr,TM)B_2$ solid solutions with TM = Hf, Nb, W, Ti, and Y. J Am Ceram Soc. 2014;97(5):1552–8.
22. Stanfield AD, Hilmas GE, Fahrenholtz WG. Effects of Ti, Y, and Hf additions on the thermal properties of ZrB_2. J Eur Ceram Soc. 2020;40(12):3824–8.
23. Baumgartner HR, Steiger RA. Sintering and properties of titanium diboride made from powder synthesized in a plasma-arc heater. J Am Ceram Soc. 2006;67(3):207–12.

How to cite this article: Smith SM II, Feng L, Fahrenholtz WG, Hilmas GE, Silvestroni L. Thermal and electrical properties of spark plasma sintered $(Ti,Cr)B_2$ ceramics. J Am Ceram Soc. 2023;106:632–638. https://doi.org/10.1111/jace.18791